

pubs.acs.org/JPCC Article

# Molecular Mechanism of Thermal Dry Etching of Iron in a Two-Step Atomic Layer Etching Process: Chlorination Followed by Exposure to Acetylacetone

Mahsa Konh, Anderson Janotti, and Andrew Teplyakov\*



Cite This: J. Phys. Chem. C 2021, 125, 7142-7154



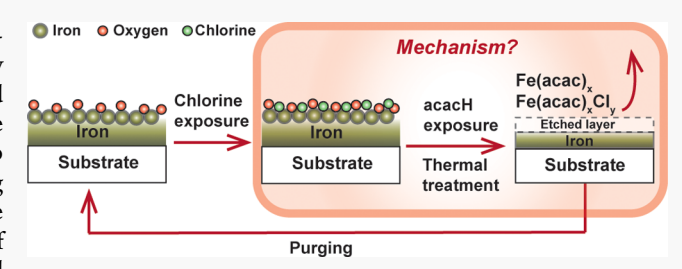
**ACCESS** 

III Metrics & More



S Supporting Information

**ABSTRACT:** Controlling thickness and morphology of transition-metal thin films used in magnetic random-access memory fabrication is a major challenge. Thermal dry etching has emerged as a method of choice for preparing the desired films; however, the mechanisms of the underlying surface processes are very difficult to assess. In this work, thermal dry etching of metallic iron by using sequential exposure to chlorine gas and 2,4-pentanedione (acetylacetone, acacH) was investigated. The mechanism of reacting acacH with chlorine-modified iron surface was studied



by following the fragments desorbing from the surface in temperature-programmed desorption experiments in half-cycle processes that compared the chlorinated, oxidized, mixed (Cl and O), and clean (sputtered) iron films. In situ Auger electron spectroscopy and ex situ X-ray photoelectron spectroscopy of each sample after each etching step confirmed that the surface is activated by chlorine and then the chlorine-containing iron species are removed from the top layer of the sample, resulting in a metallic iron surface. No etching of clean (sputtered) surface was observed with acacH. The complete mechanism of acacH reaction with chlorinated iron samples is complicated, and etch products can contain both  $Fe^{2+}$  and  $Fe^{3+}$ . However, a number of major conclusions, including the formation of surface intermediates and the final products of etching, primarily removal of  $Fe(acac)_x Cl_y$ , are inferred by comparing the results of these experiments with the computational investigation of selected surface processes using density functional theory calculations.

## 1. INTRODUCTION

The technological process involving atomically precise layerby-layer removal of materials is referred to as atomic layer etching (ALE). This approach is often used to achieve uniform ultrathin films with atomically precise thickness, especially for materials that are difficult to form by the more traditional techniques that rely on various deposition processes. The ALE process is often considered to be a reverse of the more common atomic layer deposition (ALD), with both approaches rooted in sequential self-limiting surface reactions. In ALD, each step of the process saturates the monolayer with the species of a specific chemical structure and reactivity that selectively reacts with the species of the second half of the cycle to deposit target material. In ALE, the goal is to saturate the monolayer with the species of one type and then react them with the reagent used in the second half-cycle to remove a monolayer of material. In practice, very rarely all the steps of the ALE process are fully self-limiting, which makes the experimental investigation and especially computational description of ALE even more complex. In addition, each cycle of both ALE and ALD can in general involve more than two steps.

If only temperature and pressure (concentration) are used as variables for the etching process, it is often referred to as thermal dry etching. The disadvantage of this approach is that most of the time, the process is not driven to completion thermodynamically, and the kinetic control of selected steps may be utilized. In other words, one of the half-cycles must stop at a precise surface concentration of specific species rather than rely fully on the thermodynamically driven single molecular layer saturation at reasonable processing conditions. However, the advantage of using ALE, specifically for magnetic materials, is in eliminating slow nucleation step (that often leads to surface roughening) and, moreover, in smoothing the surface of the etched film by ALE that has been reported. The thermal ALE process also eliminates the need for additional stimuli, such as plasma or ion sputtering, that are often responsible for altering the properties of the resulting surfaces. The strength of the resulting surfaces.

The majority of current ALE approaches to fabricate thin films of magnetic metals are based on a two-step scheme,

Received: November 24, 2020 Revised: March 3, 2021 Published: March 26, 2021





where the first step is kinetically controlled formation of metal oxides, <sup>4,5</sup> nitrides, <sup>6,7</sup> or chlorides. <sup>8–12</sup> The second step is then based on a selective self-limiting reaction of the produced activated layer with the co-reactant, often delivering an organic ligand that can form a volatile metal-containing compound. If the metal-containing products are volatile and thermally stable, they can be removed by simply controlling the process temperature. Sometimes, however, the second step does have to involve light sputtering <sup>13,14</sup> or plasma processing. <sup>15</sup> Overall, picking the right parameters allows in all these cases to approach the true ALE regime.

Although ALE has been used successfully in some optimized fabrication processes, 16,17 one of the questions that often remain unanswered is the mechanism of thermal dry etching. At the same time, knowing the actual chemical mechanism, the processing can be optimized for different materials and applications. Recently, there have been some substantial advances in understanding the molecular mechanisms of ALE for such materials as  $Al_2O_3^{18,19}$  HfO<sub>2</sub><sup>20</sup> and  $ZrO_2^{20}$ with the help of careful measurements of sample mass change by the quartz crystal microbalance, which can be consistent with the proposed mechanisms. Temperature-programmed desorption (TPD) has been reported for ALE of cobalt thin films. 11,21 For iron and cobalt thin films, in situ X-ray photoelectron spectroscopy (XPS) was used to probe the mechanism of metal ALE. Although the in situ spectroscopic and mass-resolved methods are by far the most informative in uncovering the mechanisms of surface processes during ALE, they are also most expensive and difficult to perform. In addition, they can rarely be performed at the same conditions as the in-operando methods. Nevertheless, for the metals such as iron described here, it is imperative to use a combination of these methods since the smallest changes in the background gas (oxygen content, humidity, etc.) may result in different surface structure and thus etching mechanisms and conditions.

Iron is one of the common transition metals used in magnetic random-access memory (MRAM) devices. MRAM devices are nonvolatile, and they exhibit improved writing speed and endurance, which attracted great interest in their properties and manufacturing.<sup>22</sup> The heart of every MRAM device is magnetic tunnel junction, which consists of at least two ferromagnetic layers isolated by a barrier layer (usually MgO). The ferromagnetic layers are commonly made of Co, Fe, Ni, Pt, and their alloys. For each of these metals, fabrication of a controlled thin film with high aspect ratio patterning encounters some difficulties, which can be overcome if the mechanism of etching process is understood at the molecular level. Our previous investigation of the mechanism of thermal dry etching of cobalt thin films revealed that diketones can be used to etch the oxidized or chlorinated cobalt.<sup>11,21</sup> It was shown that even on the oxidized cobalt surface, the proposed volatile product, Co(hfac)2, would only desorb at approximately 620 K, which is much higher than the temperature of the industrial processing conditions. The subsequent study revealed that on chlorinated cobalt surfaces, formation of less thermodynamically stable species can accelerate the etching, and the chlorine-containing species started to desorb at lower temperature (440 K). However, the challenging aspect of using halogens and diketones on a surface is that this combination makes the identification of desorbing species and thus understanding the reaction mechanism very complicated. Following all expected mass-to-charge ratios corresponding to the species that could desorb from the surface during TPD revealed that the products can contain multiligand organometallic compounds with at least some cobalt being in a +3 oxidation state.

In addition to this mechanistic investigation, the morphological changes during the etching reaction were performed using atomic force microscopy (AFM). 10,11 The roughness of the resulting surface was shown to be less than that of the original cobalt surface. The origin of this smoothing effect of ALE was examined by a simple set of theoretical investigations on a Co(100) surface model. 11 In this study, thermal dry etching of iron thin films is investigated. Given the high interest in ALE of this element, a number of previous investigations have focused on the process and offered some insights into its possible mechanisms. Of a particular interest is the work of Opila et al., 12 where it was shown that chlorination of a clean (sputtered) iron surface followed by exposure to acetylacetone (acacH) can be performed in the ALE regime with carefully chosen parameters. Importantly, that work showed that ALE could be achieved without additional surface oxidation and suggested a possible surface intermediate that could contain both Cl and acac ligands. However, the reaction mechanism was not uncovered.

Based on these previous observations, this work targets chlorination to form surface species that are less thermodynamically stable than pure metals or oxides on clean (sputtered) and oxidized surface of iron films. After activation with chlorine, acetylacetone (acacH) reacted with the chlorinated surface and the products are desorbed at elevated temperatures. The etching mechanism then investigated by TPD experiments complemented with *in situ* Auger electron spectroscopy (AES) and *ex situ* XPS, and the selected thermodynamic and kinetic aspects of the process were rationalized with density functional theory (DFT) calculations. The morphology of the surface is followed with scanning electron microscopy (SEM) and AFM.

# 2. EXPERIMENTAL AND COMPUTATIONAL METHODS

**2.1. Experimental Methods.** 100 nm iron metal (Fe) thin film was deposited on Si(100) wafers with titanium as an adhesion layer by sputter physical vapor deposition with Sputter Tool 303 (custom tool built by PVD Products) located at the University of Delaware Nanofabrication facility. The produced samples were mounted on a sample holder in an ultrahigh vacuum (UHV) chamber with the base pressure of 10<sup>-9</sup> Torr. This UHV chamber is equipped with a differentially pumped mass spectrometer (Hiden Analytical) that can detect mass-to-charge ratios up to 510 amu. Auger electron spectroscopy (ESA 100, STAIB Instruments Inc.) was used to confirm the surface composition before and after thermal etching experiments in situ. A separate set of experiments were performed with the same iron samples in a high vacuum chamber for XPS investigations. In all cases, the samples were prepared by annealing at 440 K for 40 min to remove physisorbed contaminants. For chlorinated samples, molecular chlorine gas was dosed into the UHV chamber using a homebuilt solid-state electrochemical cell based on silver chloride. Cadmium chloride was also used in this cell to increase the defect concentration and allow the cell to work continuously for extended periods of time. 23,24 The surface chlorine saturation within the experimental conditions used in this work was confirmed by AES. 2,4-Pentanedione (acacH)

(99.5%, Aldrich) was introduced into the chamber through leak valves after several freeze—pump—thaw cycles. The purity of the compound was confirmed *in situ* by mass spectroscopy. After dosing the predetermined amount of acacH into the chamber, the temperature of the sample was lowered to approximately room temperature for thermal desorption experiments. During thermal desorption, the temperature of the sample was increased linearly with a 2 K/s rate up to 720—750 K controlled by a dedicated temperature controller (Eurotherm, model 818). The desorbing fragments were followed by a mass spectrometer. The studies presented below target chlorine-containing fragments with <sup>35</sup>Cl isotope, unless specified otherwise.

Surface chemical characterization was performed *ex situ* by XPS on a K-alpha + XPS system from Thermo Scientific in the Surface Analysis Facility at the University of Delaware using an Al K-alpha X-ray source ( $h\nu=1486.6~{\rm eV}$ ) at a 35.3° takeoff angle with respect to the analyzer. High-resolution spectra were collected over the range of 20 eV at 0.1 eV/step with the pass energy of 20 eV. The survey spectra were collected over the energy range of 0–1000 eV. CasaXPS (version 2.3.16) software was utilized to analyze all data. To calibrate the XPS scale, the carbon peak was set at 284.6 eV.

AFM images were acquired under the tapping mode with a J-scanner scanning probe microscope (Multimode, NanoScope V). The sensing tips (aluminum coated, BudgetSensors) have a resonant frequency of 300 kHz and a 40 N/m force constant. The images were processed with Gwyddion software.

A Zeiss Auriga 60 scanning electron microscope at the W. M. Keck Electron Microscopy facility at the University of Delaware was used for all electron microscopy investigations. The accelerating voltage was 2 kV with a secondary electron (in-lens) detector at the working distance of 4.0 mm.

**2.2. Computational Modeling.** Selected DFT calculations for the molecular species were performed using the Gaussian 09 suite of programs<sup>26</sup> in order to compare the stability of several fragments containing acacH and chlorine attached to iron atoms. The geometry was optimized with the B3LYP functional<sup>27,28</sup> and the 6-311+G(d,p) basis set<sup>29</sup> including Grimme's D3 dispersion correction.<sup>30</sup>

The calculations describing possible pathways of surface etching on different Fe(100) surfaces were carried out using the projector augmented wave method and spin-polarized DFT + U, as implemented in the Vienna Ab initio simulation package (VASP) code. 31,32 The U-I parameter 33 of 4 eV for the Fe 3d orbitals was used in all calculations. A supercell with a slab geometry based on the Fe body-centered cubic (bcc) structure was constructed with five layers of atoms representing the most stable Fe(100) face of the structure, with each layer consisting of 16 iron atoms  $(4 \times 4)$ , as shown in Figure 1. For all the models describing adsorbed species or their removal, the top two layers of 32 Fe atoms were set to relax, while the rest of the atoms were fixed to simulate the underlying atomic layers in the bulk system. A vacuum spacing layer of 17 Å in z-direction and the  $4 \times 4$  in-plane cubic unit cell were found sufficient to minimize the intermolecular interactions between periodically repeated neighboring cells. The calculated lattice parameter of 2.866 Å for bcc-Fe is in good agreement with the experimental value of 2.858  $\hbox{Å.}^{34}$  The cutoff energy for the planewave basis set was 350 eV, and forces on each atom that could relax were minimized to less than 0.01 eV/Å. The k-space integrations were performed using a 2 × 2 × 1 Monkhorst-Pack mesh for the slab

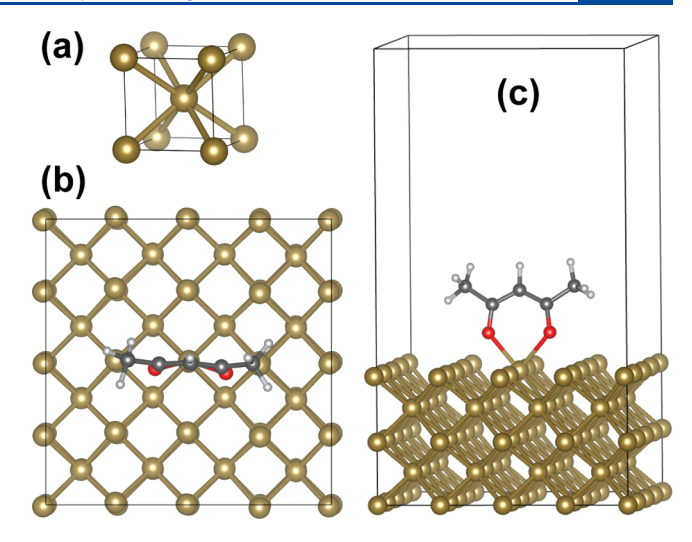


**Figure 1.** Ball-and-stick model for the (a) cubic unit cell of bcc-Fe and the slab model used in the DFT + U calculations: (b) top and (c) perspective view of the Fe(001) slab with an attached acac ligand.

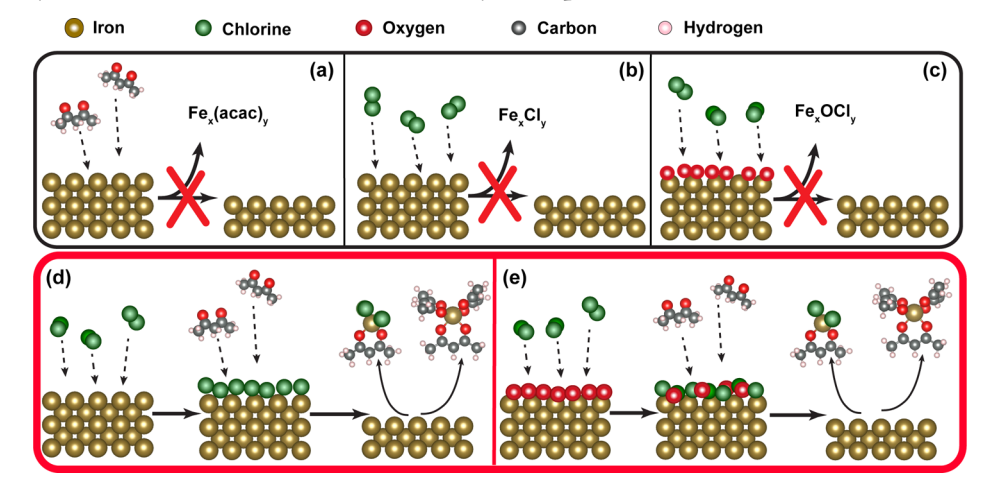
calculations, which is equivalent to a  $16 \times 16 \times 16$  mesh for the 1-atom primitive cell. Tests were performed increasing the k-mesh for the slab calculations. The removal energy of an iron adatom changed from 3.25 to 3.20 eV by increasing the k-mesh from  $2 \times 2 \times 1$  to  $4 \times 4 \times 1$ . These calculations were conducted to understand the reaction pathway of removal of an iron atom from the surface with or without organic ligand or chlorine. To do so, the energy required for the reactions that produce a volatile compound containing an iron atom with chlorine, acacH ligand, or a combination thereof was obtained.

#### 3. RESULTS AND DISCUSSION

**3.1.** Investigation of Surface Chemistry following Sequential Chlorine and acacH Exposures. The goal of this work is to follow the desorption of iron-containing products in half-cycles of the ALE process with chlorine and acacH to understand the underlying mechanism. The premise of the experiment on the Cl-covered iron is based on previously investigated ALE steps described by Opila et al. Scheme 1 describes the general approach and summarizes the reactions that we follow.

The top line in Scheme 1 lists the processes that are not expected to lead to the ALE. Based on the previously reported studies utilizing diketones for metal etching, 10-12,21 ALE chemistry does not appear to work with diketone being the only reactant and is only possible with oxygen or halogen present on a surface. That is indeed the case in the present investigation. No Fe-containing desorption products were recorded to desorb from a clean (sputtered) iron surface exposed to acacH within the experimental conditions tested. Figure S1 in Supporting Information section summarizes several key fragments that were followed experimentally. In fact, no desorption of any iron-containing products was found, and, similarly to the reactions of diketones with cobalt, 11,21 the only process was acacH decomposition. Some of the acacH desorption was observed above 600 K; however, the very small signal at that high temperature may be influenced by the desorption from the heating elements in the experimental setup. The desorption of iron chlorides from chlorinated surface, oxides from oxidized surface, or oxychlorides from oxidized iron surface exposed to chlorine gas would require

Scheme 1. Summary of Processes on Iron Surface Caused by Adsorption and Reactions of Chlorine and acacH<sup>a</sup>



"No iron-containing fragments expected to desorb by using only diketone or chlorine from the clean (sputtered) iron surface (a,b) or by dosing only chlorine on the partially oxidized iron surface (c). The ALE process occurs when diketone reacts with chlorinated or oxidized iron surface, and examples of ALE product in these cases are Fe(acac)Cl and Fe(acac)<sub>3</sub> (d,e).

very high energy, above 330 kJ/mol, 35-38 according to the Redhead method; these processes could only occur above 1000 K and would be limited by sublimation. This is consistent with the previously observed desorption of Co-containing species from chlorinated cobalt surface at 625 K. 11 In other words, for ALE to be practical, additional ligands would be necessary, as suggested in the bottom line of Scheme 1, and these reactions will be the focus of the current work.

Starting with the oxidized or halogenated surface is a prerequisite to achieve successful etching since oxygen or halogen can lead to the formation of volatile byproducts (such as H<sub>2</sub>O or HCl) and simultaneously help accommodate the acetylacetonato groups onto the surface that ultimately should aid in removing iron-containing species. In the current study, multiple sets of experiments with clean, oxidized, and chlorinated surfaces are performed to explore the possibility of thermal etching of iron thin films using acetylacetone. Each surface was annealed at 440 K for 40 min to remove physisorbed impurities and reduce carbon contamination.

In order to evaluate the state of the surface during ALE half-cycles, XPS investigation, even though not performed in situ, can provide crucial information. For example, the chemistry of acacH on iron is clearly different if oxidized iron is used instead of a clean surface. Figure 2 shows high-resolution Fe 2p XPS data for oxidized iron thin films. As the starting film is saturated with acacH, the intensity of the  $2p_{3/2}$  peak at 706.7 eV corresponding to metallic iron<sup>39</sup> decreases. However, annealing at the elevated temperature ( $\sim$ 750 K) appears to reclaim metallic iron by either reduction process or by removing the possible volatile iron-containing species, as shown in Figure 2c, and the focus of this work will be on chlorine-based surface processes.

The investigation of the ALE mechanism was performed on chlorinated iron thin films that were intentionally oxidized. If the iron surface is not sputtered, it is partially oxidized to start with. The chlorine gas was dosed onto the surface at 373 K using an *in situ* solid-state chlorine source for 40 min at 3  $\mu$ A. The organic compound, 300 L acacH, was introduced to the surface at 440 K through a leak valve. The chlorination temperature of 373 K was chosen as the lowest possible temperature for chlorination, and 440 K was used for acacH

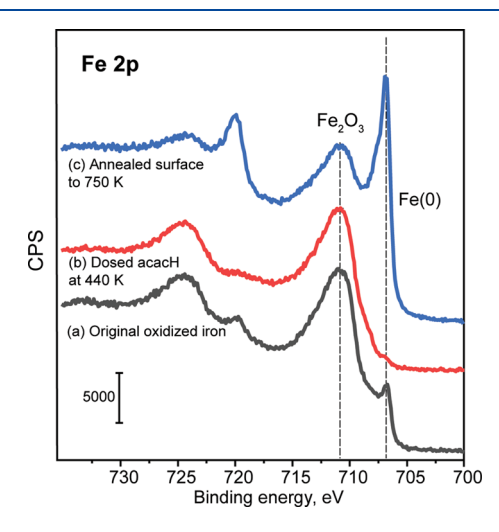


**Figure 2.** High-resolution XPS investigations of the Fe 2p spectral region for (a) original oxidized iron, (b) iron sample exposed to acacH at 440 K, and (c) sample in red annealed at 750 K.

dosing as it was the optimized temperature for iron ALE reported previously by Opila et al. 12 As shown in Figure 3, the chlorinated partially oxidized surface is compared to the same sample but after dosing acacH and briefly annealing at 720 K. As the Fe 2p binding energy region suggests, the signature of metallic iron appears after annealing, same as for oxidized iron thin films. The peak at higher binding energy, 710.4 to 710.8 eV, is likely associated with a combination of iron(II) in FeCl<sub>2</sub> and iron(III) in Fe<sub>2</sub>O<sub>3</sub>.<sup>40</sup> However, after heating at 720 K, the shape of the peak changes, and its position shifts slightly to higher energy, which is more consistent with the presence of Fe<sub>2</sub>O<sub>3</sub>. This is also fully consistent with chlorine removal, as shown in Figure 3. The choice of 440 K adsorption temperature for acacH is based on the previously confirmed temperature needed for ALE to occur at UHV conditions with a combination of chlorine gas and acacH. 12 That is also the temperature of a brief annealing in all the experiments reported here to remove surface impurities that are weakly physisorbed on samples.

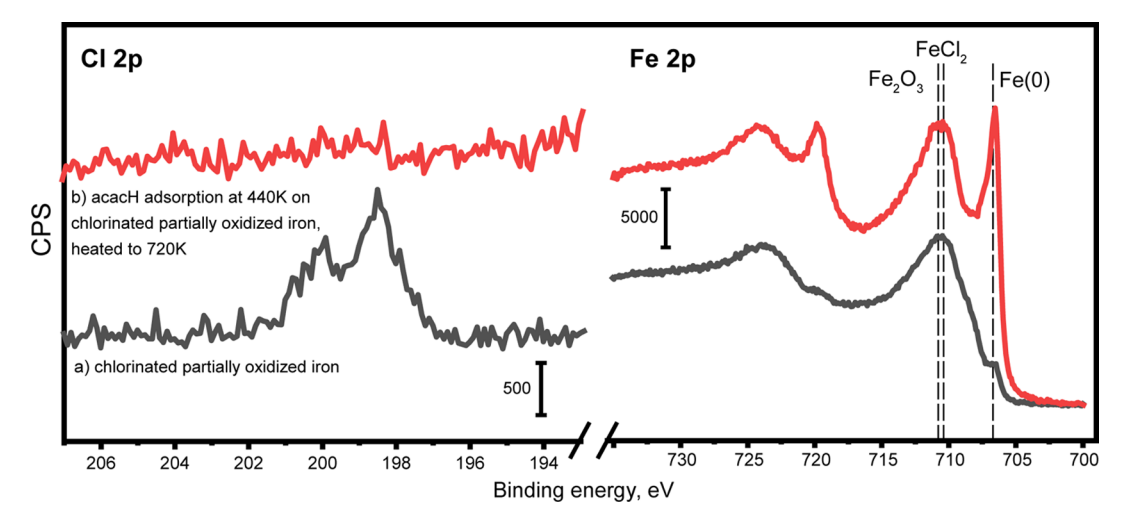
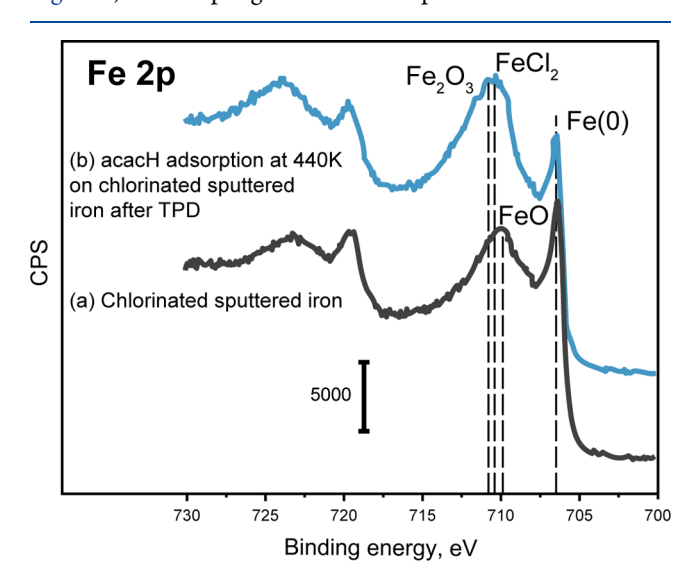


Figure 3. High-resolution XPS investigations of Cl 2p and Fe 2p spectral regions for (a) chlorinated partially oxidized iron and (b) chlorinated partially oxidized iron sample exposed to acacH at 440 K and annealed at 720 K.

It is interesting to note that even though iron ALE process analysis reported by Opila et al. 12 does report oxygen-free environment, in practice iron surface is expected to be at least partially oxidized in any commercial processing, unless it is performed at UHV conditions. Thus, the comparison between chlorination on clean and oxidized iron surfaces is important to understand the chemistry behind the etching process. To address this idea, an iron sample was sputtered with argon ions in the UHV chamber to remove oxygen from the surface, as confirmed by AES, then the clean surface was exposed to chlorine and acacH followed by heating at 720 K. As shown in Figure 4, the Fe 2p region for this sample is different from iron



**Figure 4.** High-resolution XPS investigations of the Fe 2p spectral region for (a) sputtered clean iron followed by chlorination and (b) chlorinated clean (sputtered) iron sample exposed to acacH at 440 K and heated to 720 K.

signature of chlorinated partially oxidized iron (Figure 3). Here, the peak corresponding to metallic iron did not change after heating (after TPD) but the oxidized peak shifted from Fe(II) in FeO to a position consistent with Fe(II) in FeCl<sub>2</sub> and Fe(III) in Fe<sub>2</sub>O<sub>3</sub>. This is especially important to understand since all the XPS investigations are performed *ex situ* after a

brief (several minutes) exposure to ambient. In other words, once the surface is oxidized, its exposure to chlorine gas does introduce chlorine to the surface but does not substantially affect the iron oxidation state. However, a sputter-cleaned iron surface exposed to chlorine appears to be protected toward further oxidation as metallic iron signature is clearly observed. Following half-step of the ALE process, the Fe(0) peak remains prominent, as confirmed by the results presented in Figure 4.

Based on the results of the XPS investigation, it can be concluded that oxidation or chlorination or both are needed to control the reactivity of the surface with acacH, that the clean iron surface does not form volatile iron-containing products, and that the introduction of acacH at appropriate conditions (approximately 440 K) does lead to the changes in the oxidation state of surface iron. The big question, however, is if these changes led to the desorption of iron-containing products within the reasonable temperature range that would be needed for ALE.

In order to address this question, a set of TPD experiments starting with various modified iron surfaces was recorded. As the results of this work are discussed, it is important to understand that the desorption patterns of different products must be considered in a context of the temperature regime of each experiment. For example, since all the samples were initially briefly annealed at 440 K, it is not expected that any products would desorb below this temperature, unless surface chemistry is altered by dosing acacH. If acacH is dosed at room temperature, this may not lead to the formation of kinetically hindered volatile products. Finally, if the acacH is dosed at 440 K but the TPD starts at room temperature, it is possible that the products of the ALE process have already desorbed at that point. Despite such complications, this technique is very valuable if it can confirm temperature-dependent evolution of any iron-containing process at the temperatures where feasible ALE processing can be performed.

Figure 5 shows the summary of the results of thermal desorption study of chlorinated and partially oxidized iron thin films following acacH adsorption at room temperature (RT) and at 440 K. According to the mechanism previously proposed for cobalt, <sup>11,21</sup> we could expect to observe the desorption of Fe(acac)<sub>2</sub> or Fe(acac)<sub>3</sub> as possible products. For the sputter-cleaned iron surface exposed to acacH either at 440

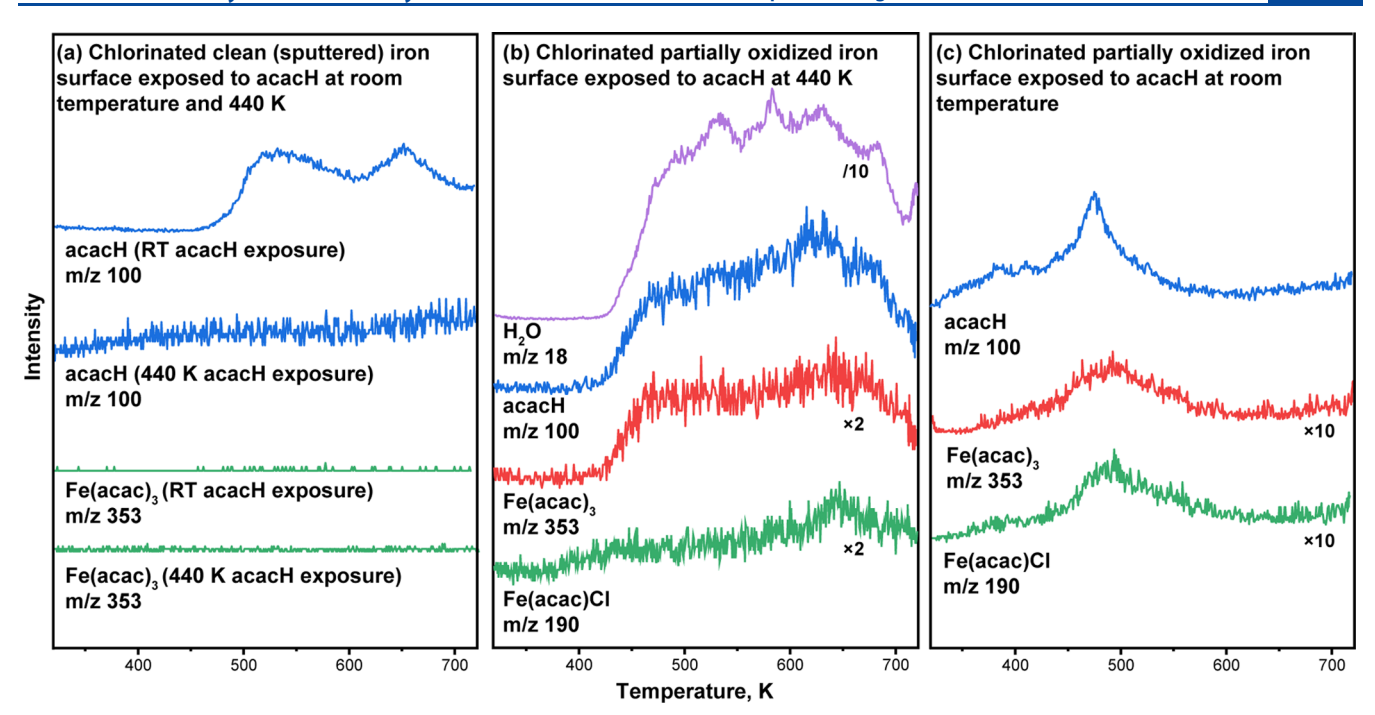


Figure 5. Summary of TPD studies of (a) chlorinated clean (sputtered) iron thin films exposed to acacH at 440 K and at room temperature and (b) chlorinated partially oxidized iron thin films exposed to acacH at 440 K and (c) at room temperature.

K or at room temperature, no Fe-containing desorption products are observed (Figure 5a). Moreover, no acaccontaining products (other than acacH desorption that starts around 500 K) are recorded, suggesting that the primary pathway for acacH interaction with clean iron following TPD would be desorption or decomposition. However, it is important to note that the previous studies of iron ALE with the combination of Cl<sub>2</sub> gas and acacH did report the process to proceed at 410 K.<sup>12</sup> In other words, our TPD investigations start with a surface at room temperature, while the in-operando studies appear to be kinetically driven. This observation will be aided by computational investigations below, but it is important to note that in the case summarized in Figure 5a, acacH dosed at room temperature onto a chlorinated surface appears to only lead to the desorption of some acacH at elevated temperatures in a TPD experiment, while if the same experiment is performed with dosing acacH at 440 K, no desorption of any products is registered. In fact, no ironcontaining products of any kind were recorded for the experiments where acacH was dosed at 440 K. Of course, this does not mean that the reactions do not occur. It just means that any reactions removing Fe- and acac-containing products occur at approximately 440 K, which is fully consistent with the findings of Opila et al.1

TPD results on the partially oxidized and pre-chlorinated surface (Figure 5b,c) clearly show that the TPD technique is indeed capable of following Fe-containing products, with several fragments containing both Cl and acac ligands desorbing from the surface. For example, as shown in Figure 5b, the evolution of the Fe(acac)Cl fragment (proposed in the previous studies as the possible surface intermediate)<sup>12</sup> from the chlorinated partially oxidized iron surface exposed to acacH at 440 K is recorded to start just around the temperature of this initial acacH dose. In this TPD investigation, this fragment (that can also be a part of more complex species) appears to be minor compared to the

Fe(acac)3, which also starts to desorb around the same temperature, together with H<sub>2</sub>O and some molecularly desorbing acacH. On the other hand, if the same experiment is repeated with dosing acacH at room temperature, same Fecontaining and acac-containing fragments are clearly observed to start desorbing well below 440 K, around 400 K, suggesting that the comparison of the two sets of experiments presented in Figure 5b,c demonstrates that the results of a kinetically driven process can still be observed by exploring different adsorption temperatures of one of the adsorbates in selflimiting ALE processes. One problem with further quantification of the observed processes and the specific products desorbing during ALE or in TPD experiments is the complexity of the products. If in some of the previous work on cobalt ALE, 11,21 the mass spectra of the desorbing products of the reaction could be compared with the mass spectra of specific individual compounds from the literature, in the case of iron, it appears to be nearly impossible since the products of the process are expected to follow the overall formula Fe<sub>x</sub>Cl<sub>y</sub>(acac)<sub>z</sub> and could also be oxidized because of the presence of surface oxygen. Nevertheless, some of the suggestions for possible products can be substantiated by computational investigations described further.

To summarize this part of the work, it can be inferred from the TPD studies that the iron ALE products are a complex mixture of compounds containing multiple ligands (acac and chlorine) with iron in +2 or +3 oxidation states, which is consistent with the indirect ex situ XPS investigations presented above. Based on the previously published cracking patterns for  $Fe(acac)_2$  or  $Fe(acac)_3$ ,  $^{41,42}$  it appears that the recorded TPD traces are not consistent with the spectra of these pure compounds. Given that iron chlorides are not expected to desorb until their sublimation points, it is most likely that we would have a combination of acac and chlorine attached to the iron center rather than  $Fe(acac)_2$  or  $Fe(acac)_3$  present in this mixture. As noted above, desorption of water

with m/z = 18 and acacH with m/z = 100 was also observed at about the same temperature (starting at 440 K). Other fragments corresponding to cracking patterns of possible desorbing compounds, such as Fe<sup>35</sup>Cl (m/z = 91) and <sup>37</sup>Cl, were also detected (not shown); however, each of those are difficult to interpret since they overlap with a number of possible hydrocarbon and background species (e.g.,  $m/z^+ = 91$ could correspond to C<sub>4</sub>H<sub>8</sub>Cl). Another conclusion brought by the TPD investigation is that the temperature interval between room temperature and 440 K appears to be crucial in determining the efficacy of surface reactions and thus the possibility of ALE processing. The observations do confirm that the addition of acacH to the chlorinated iron surface (either clean or oxidized) can be controlled kinetically. Apparently, the process is very inefficient if acacH is dosed at room temperature; however, combined with the previous detailed work on Opila et al., 12 the process for monolayer desorption of iron-containing products is complete if acacH is dosed at 440 K.

Along with the TPD investigations and to confirm *ex situ* XPS experiments, surface elemental analysis was also performed with *in situ* AES. Monitoring the surface before and after the etching process clearly shows that chlorine present on the surface before acacH exposure following by the TPD experiment is then completely removed after heating at 720 K, as summarized in Figure S2 in Supporting Information section. This observation is consistent with the proposed mechanism where iron atoms from a surface modified by oxygen and/or chlorine are removed from the surface at elevated temperatures and mainly metallic iron remained after the first cycle of the thermal dry etching process.

**3.2. Changes in Surface Morphology.** It was shown previously that exposure of organic ligand on the metal surface may increase its roughness. However, following thermal annealing and etching of the surface will result in smoothing the surface (although pit formation was also reported at highly elevated temperatures). Here, we examine the surface morphology by SEM complemented by AFM investigation. Consistent with the previous studies, acacH adsorption on the oxidized iron sample resulted in somewhat rougher surface, as can be observed by comparing images (a,b) in Figure 6,

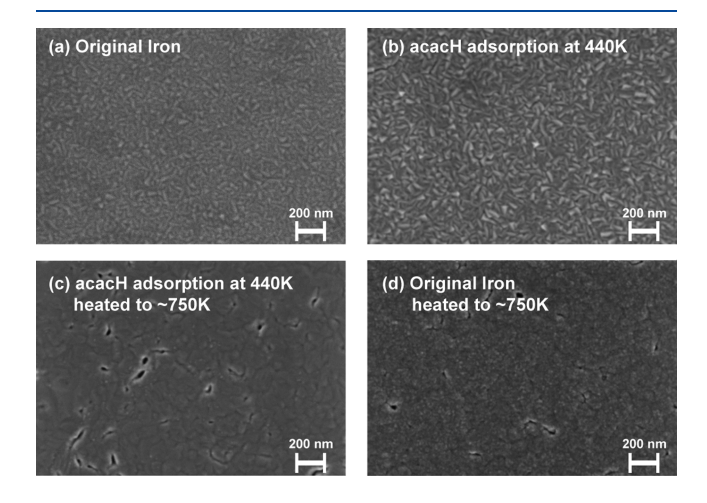


**Figure 6.** SEM images of iron thin films: (a) pristine iron thin film; (b) acacH adsorption at 440 K onto iron thin film; (c) annealing the iron thin film exposed to acacH to 750 K; and (d) annealing the iron thin film (no acacH dose) to 750 K.

possibly due to complex surface reconstruction and formation of various surface species. Following heating at elevated temperatures, the surface becomes smoother, as shown in Figure 6c, which can be explained by desorption of produced fragments from the surface (etch). Pit formation is also observed at high temperature, similar to that observed previously for cobalt films; 21 however, this process is decoupled from the ALE, as demonstrated by the results in Figure 6d, where the same starting iron surface is heated to the same elevated temperature without any chemical treatments. The AFM investigation shown below demonstrates that the formation of the pits can be avoided if the surface temperature is kept under 720 K. Thus, based on the images presented in Figure 6, it can be immediately concluded that the pits are originated from thermal treatment of the films themselves, while the smoothing effect is solely the consequence of the etching process.

In order to investigate this process at higher spatial resolution, AFM is used to study the surface roughness as it evolves during the thermal dry etching of iron thin films with and without halogenation step. Figure 7 is a summary of AFM images for the iron sample at different stages in etching process. Following a saturating exposure of acacH to the partially oxidized iron surface at 440 K, the (root mean square) roughness increases slightly from 3.8 to 4.3 nm. However, heating the surface to elevated temperature (above 700 K) will result in the smoother surface (rms = 2.7 nm) which is consistent with the previous observations in cobalt etching investigation.<sup>11</sup> The smoothing can be caused by the removal of Fe(acac), Cl, fragments, which may be preferential on defect sites, such as adatoms, kinks, or steps. Figure 7e examines the iron surface after chlorination, which shows no substantial roughness changes compared to the pristine iron surface. Following the exposure of acacH onto a chlorinated iron sample and heating at elevated temperatures (~720 K), no pit formation is observed. Thus, if the temperature is kept under 720 K, a smoothing effect without pit formation can be confirmed. It places the upper limit for any treatment for the iron films of the type used in this work.

3.3. Computational Investigation of the Energetics of **Iron ALE Process.** The experimental studies presented above discover a very complex chemistry behind iron ALE and only provide a glimpse of the entire process. Nevertheless, one of the common themes in variations of the iron ALE on iron surfaces is the requirement for at least two chemical components. Whether the surface contains only chlorine or chlorine and oxygen, it definitely affects the chemical process; however, addressing all the possible steps would be beyond the scope of this work. Nevertheless, computational investigation can help one understand the role of chlorine in stimulating the ALE process on iron. Since Cl and acac ligands are common in iron chemistry, they will be the focus of a set of computational work described below, and the role of surface-bound chlorine atoms will be explored. That leaves investigations of the effects of surface oxidation and coverage of surface species for further work.

To corroborate the hypothesis of the formation of  $Fe(acac)_xCl_y$  species on chlorinated iron surfaces reacting with acacH, a set of quantum mechanical calculations was performed. First, a set of plausible overall reactions that could occur on the chlorinated iron surface following exposure to acacH was investigated based on the simple molecular species assuming that the stable  $Fe^{2+}$ - and  $Fe^{3+}$ -containing products

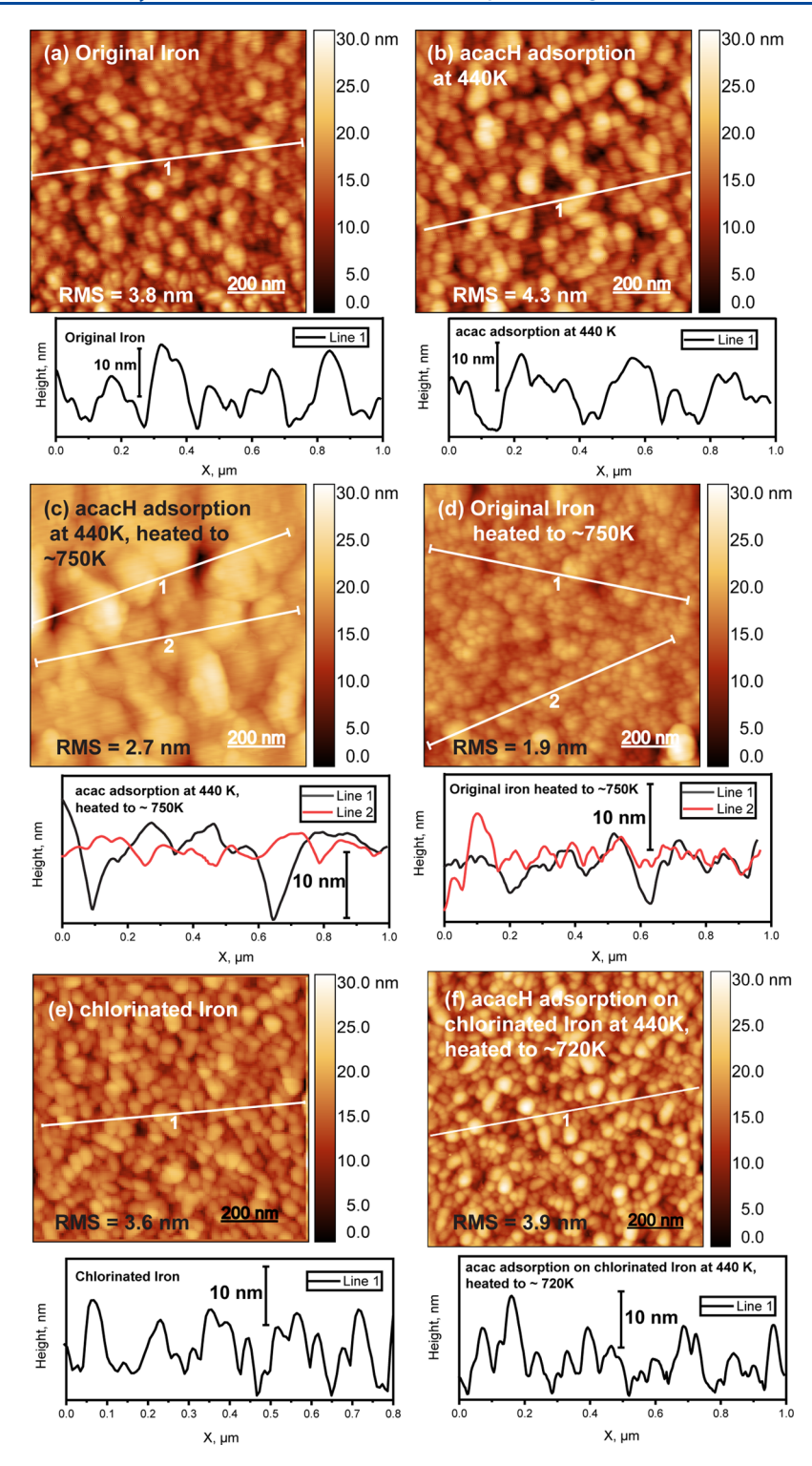


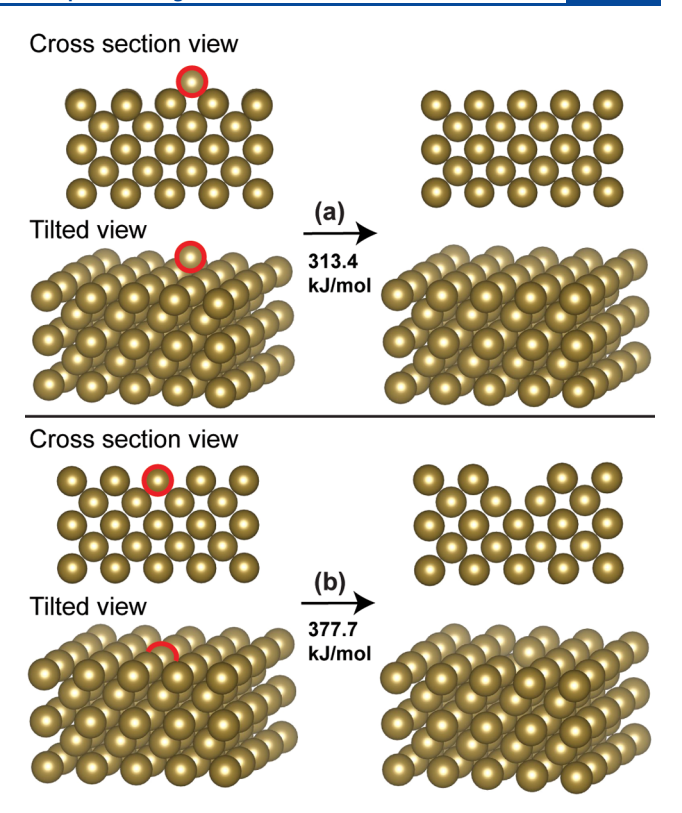
Figure 7. AFM images of iron thin films: (a) original iron thin film; (b) acacH adsorption at 440 K; (c) annealing the iron thin film exposed to acacH at 750 K; (d) original iron thin film (without acacH) heated at 750 K; (e) chlorinated iron thin film; (f) sample in (e) exposed to acacH at 440 K and heated at 720 K.

Table 1. Reaction Energy Comparison for Fe<sup>2+</sup> and Fe<sup>3+</sup> Compounds with acacH and Chlorine

| reaction investigated                 | reaction energy (kJ/mol) | reaction investigated                   | reaction energy (kJ/mol) |
|---------------------------------------|--------------------------|---|--------------------------|
| $Fe^{2+}$                             |                          | $Fe^{3+}$                               |                          |
| $FeCl_2 + 2acacH = Fe(acac)_2 + 2HCl$ | -178.6                   | $FeCl_3 + 3acacH = Fe(acac)_3 + 3HCl$   | -229.1                   |
| $FeCl_2 + acacH = Fe(acac)Cl + HCl$   | -98.6                    | $FeCl_3 + 2acacH = Fe(acac)_2Cl + 2HCl$ | -190.5                   |
|                                       |                          | $FeCl_3 + acacH = Fe(acac)Cl_2 + HCl$   | -136.3                   |

evolving during the ALE process could only possibly contain Cl and/or acac ligands and that the starting point would be FeCl<sub>2</sub> or FeCl<sub>3</sub>. It is understood that the starting point of the ALE may be quite different from dichlorides or trichlorides, as will be discussed below; however, this initial summary would help one evaluate the possibility of formation for different etching products. Table 1 summarizes this set of studies on the formation energies for the compounds leading to the evolution of possible Fe<sup>2+</sup>- and Fe<sup>3+</sup>-containing products because of the etching process based on these DFT calculations. The first observation is that all the possible reactions leading to the formation of iron fragments that contain acac ligand starting from chlorinated iron species are thermodynamically feasible since all these processes should be exothermic. The second important observation is that the thermodynamic driving force for such substitution is more substantial for Fe3+-containing compounds than for the fragments based on Fe2+ species. In the context of surface chlorination, it is possible that both Fe<sup>2+</sup> and Fe<sup>3+</sup> could be present before the ALE process with acacH. The reaction energies leading to the formation of Fe(acac)<sub>2</sub> and Fe(acac)Cl from FeCl2 are predicted to be -178.6 and -98.6 kJ/mol, respectively. On the other hand, Fe(acac)<sub>3</sub>, Fe(acac)<sub>2</sub>Cl<sub>1</sub> and Fe(acac)Cl<sub>2</sub> can be formed from FeCl<sub>3</sub> in exothermic processes gaining 229.1, 190.5, and 136.3 kJ/mol in stability, respectively. Overall, it appears that the formation of Fe(acac), compounds is more likely compared to Fe(acac)<sub>x</sub>Cl<sub>y</sub> fragments. For instance, the energy needed to evolve Fe(acac)<sub>2</sub> is about 80 kJ/mol lower than that for Fe(acac)Cl. The reaction leading to Fe(acac)<sub>3</sub> formation is more exothermic than those leading to the formation of Fe(acac)<sub>2</sub>Cl or Fe(acac)Cl<sub>2</sub>. However, it is expected that the actual reaction mechanism may be influenced by substantial kinetic contribution of the process since multiple acac ligands are required to form some of the species, as listed in Table 1. In addition, the process itself may involve changes in the iron oxidation state at different steps, making the overall mechanism even more difficult to assess. For example, it has been shown previously that carboxylic acids can reduce the oxidation state of copper upon adsorption on copper oxides, 43 and that exposure of cobalt to hfacH also reduces the cobalt oxidation state.<sup>21</sup> It is also possible that the formation of mixed products is a result of a reduction/reoxidation process that leaves Fe(0) on a surface and removes Fe(2+) as Fe(3+). Further work is needed to understand all these possibilities; however, this set of computational investigations certainly takes a step toward understanding the complicated processes

To understand how the simplistic molecular study translates into the surface reaction mechanisms, the proposed iron thin films etching was also evaluated by periodic structure calculations. The Fe(100) was chosen as a representative iron surface since it is the most thermodynamically stable one and has been used to illustrate iron material reactivity in the computational work before. Two different Fe(100) starting surfaces were chosen to follow as proposed models: a flat terrace surface and the same surface with an adatom. This combination allows for a comparison of energetics for an ideal and defective surface structures. The comparison of energy needed for removal of one iron atom from each surface is shown in Figure 8. The energy required to remove one defect iron atom (adatom) is 64.28 kJ/mol lower than that required for the removal of an iron atom from the terrace site. The computed energies are fully consistent with the experimentally



**Figure 8.** DFT investigation of removing (a) iron adatom from a (100) iron surface and (b) removing a terrace iron atom from the same surface.

observed Fe-Fe bond strength,<sup>36,46</sup> and the lower exothermicity of the removal of an adatom compared to that for the terrace atom is expected.

As it was suggested above based on the experimental results, the etch products could contain chlorine ligand, acac or a combination of both. Figure 9 presents a list of surface processes, with corresponding energy requirements, leading to the formation of Fe(acac)<sub>2</sub> and Fe(acac)<sub>3</sub> starting with acac adsorbed on a surface with an adatom (a) and an ideal terrace (b). Two likely configurations were considered for acac ligand binding to each surface: monodentate and bidentate. Bidentate configuration of acacH ligand is substantially more stable than the monodentate configuration, and as the numbers shown on Figure 9 suggest, removal of an iron atom with a bidentate acacH ligand initially attached to it in all cases is quite unfavorable. However, if the starting point is a monodentate acac, the energy requirements for a removal of corresponding iron atom bound to such a ligand, are profoundly less demanding. Additional observations based on the results summarized in Figure 9 are (1) that the removal of the adatom is much more favorable than the same process removing an atom from the terrace site, and (2) the processes involving Fe3+ and Fe2+ are very similar thermodynamically, if comparison is made for the properly normalized number of species.

The results presented in Figure 10 explore the same trends as the ones shown in Figure 9 but for chlorinated surface species. As shown in Figure 10a, chlorine atom was placed on the adatom to be removed from the surface as FeCl<sub>2</sub> or FeCl<sub>3</sub>. The same balanced reactions were examined for adsorption of chlorine atom on the terrace iron surface, as shown in Figure 10b. Based on the comparison of the results in Figures 9 and

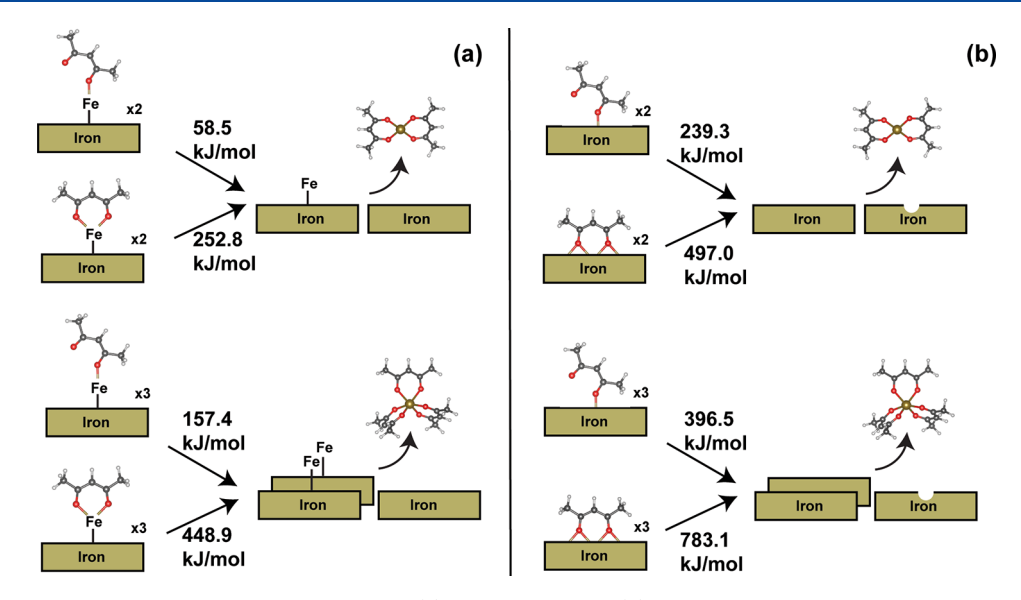


Figure 9. DFT calculations for energies required to remove (a) iron adatom and (b) iron atom from a terrace site based on plausible binding configurations of adsorbed acac ligands on the Fe(100) surface with an adatom and a flat Fe(100) surface, respectively.

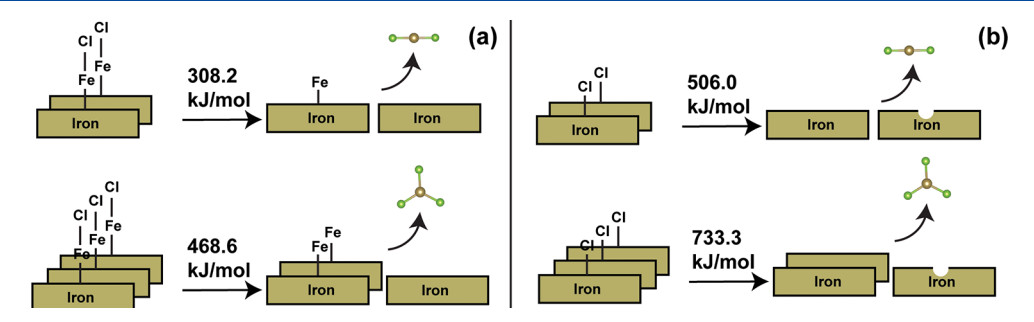


Figure 10. DFT calculations for energies required to remove (a) iron adatom and (b) iron atom from a terrace site based on plausible binding configurations of adsorbed Cl on the Fe(100) surface with an adatom and a flat Fe(100) surface, respectively.

10, it can be immediately inferred that the removal of a chlorine-bound iron fragment is very energetically demanding, especially compared to that of the species involving a monodentate acac ligand, as depicted in Figure 9.

As discussed above, removal of an iron atom from the chlorinated iron surface using the acac ligand is more complicated than a simple reaction that would produce Fe(acac)<sub>2</sub> or FeCl<sub>2</sub>. Our TPD experiments showed that other products with Fe<sup>2+</sup> and Fe<sup>3+</sup> containing both chlorine and acac ligands may also evolve from the surface during the etching process. Figure 11 shows the viable reactions to form products containing both acac and chlorine ligands. A single chlorine atom bound to a terrace site iron atom is considered in this figure as a starting point of the process. It is expected that surface dichloride or a chlorine atom attached to an iron adatom would favorably affect the thermodynamics of the overall reaction. Based on the energies required for each of these balanced reactions, we can clearly confirm that the energetics of ALE reactions starting with terrace-bound chlorine and bidentate acac is prohibitively expensive. However, producing Fe(acac)Cl, Fe(acac)2Cl, and Fe(acac)Cl<sub>2</sub> starting with a monodentate acac ligand is much more feasible.

All these model studies are very consistent with the observation of a smoothing effect of ALE as in all these schemes, the energy required to remove an adatom is substantially lower than that needed to remove an iron atom

from a terrace site. Much more interesting though is the observation that if the most thermodynamically stable bidentate structure of the surface-bound acac ligand is considered, the energetics of the Fe-containing product removal is almost as demanding as that without the help of the acac ligand (which is not observed experimentally). However, if the formation of the monodentate acac is possible, the energetics becomes much more amenable for the reaction leading to the iron-containing product removal. This observation leads us to think that there may be a disconnect between the numerous current computational investigations of the ALE process and the realistic processing conditions. The majority of the computational studies of the diketonate ligands participating in the metal ALE start with the most thermodynamically stable bidentate structure 11,47,48 and find it thermodynamically impossible at reasonable processing conditions to form a metal-containing product that could be removed from the terrace site of the surface. However, in realistic processing conditions, at reasonably high pressures, the kinetic factors and surface crowding by the ligands could easily lead to the formation of stable monodentate diketonate ligands as dominant surface species (even if there is a presence of stable bidentate ligands) that could fundamentally change the energy landscape for analysis of ALE schemes.

Of course, further investigations are required to understand the kinetic barriers of the processes considered and to follow the role of mixed ligands, mixed surface configurations, the role

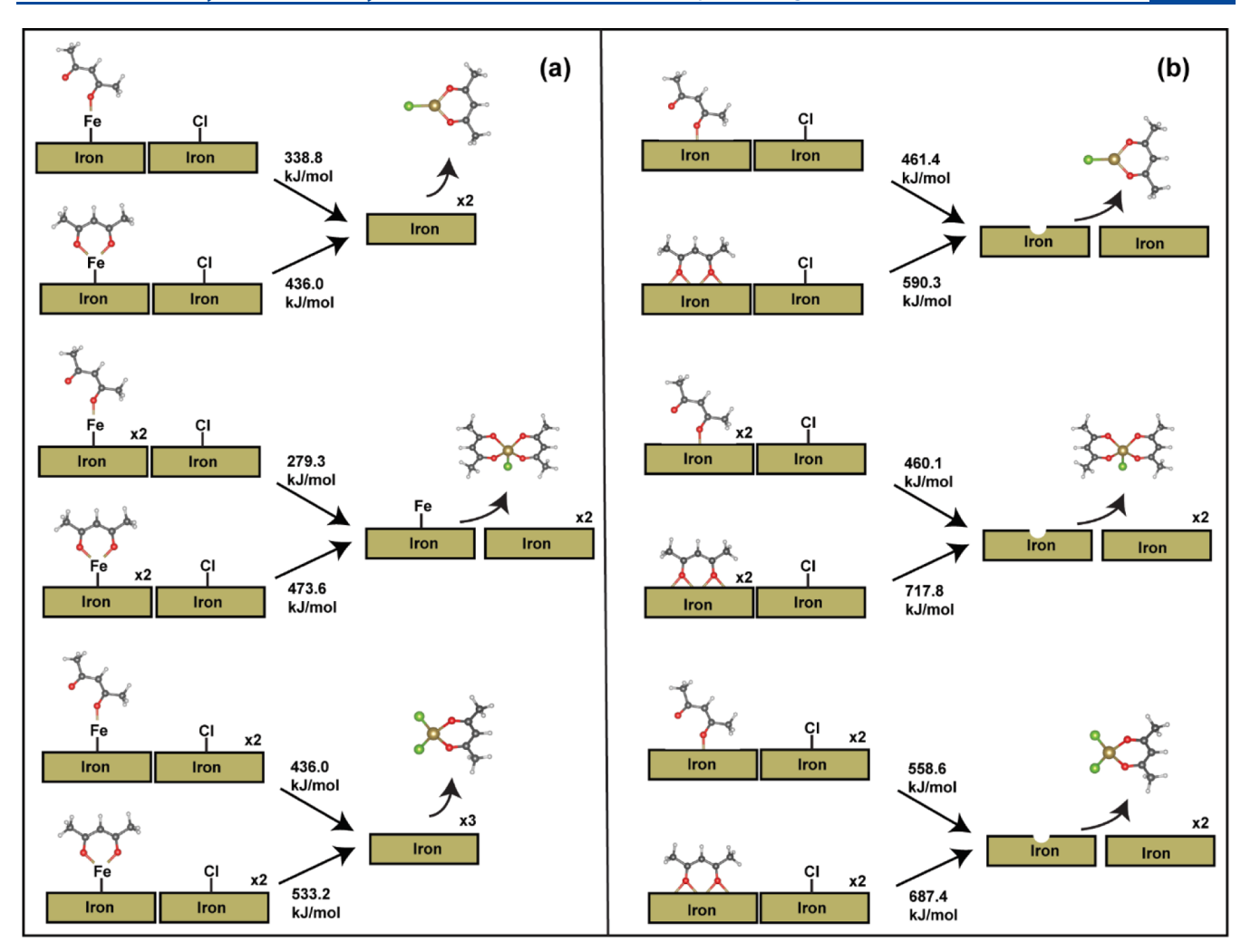


Figure 11. DFT calculations for energies required to remove (a) iron adatom and (b) iron atom from a terrace site based on plausible binding configurations of adsorbed Cl and acac ligands.

of oxygen, and surface oxide formation in realistic ALE conditions. However, these fundamental studies need to involve realistic conditions and high surface concentrations of ligands, which may require considering the models that are not the most thermodynamically stable ones for low-coverage regimes.

#### 4. CONCLUSIONS

The mechanism of thermal dry etching of iron thin films was investigated using spectroscopic and microscopic techniques along with the selected computational work. It was shown that in order for the ALE process to work, at least two etching components have to be used (acacH and chlorine in this work) and that surface oxidation does affect the mechanism of this process. The mechanisms of the surface reaction pathways studied by TPD shows that there are several products containing both chlorine and acac ligands, and that at reasonable thermal regimes, they start desorbing within the temperature range required for realistic ALE schemes. Microscopy studies showed that the etching process does not lead to roughening of the surface, if the etching products are removed at elevated temperatures; however, heating the surface above 720 K leads to pit formation. Among possible surface intermediates, the monodentate acetylacetonate may be able to substantially lower the energy cost for ALE

processes and should be considered further in computational studies.

#### ASSOCIATED CONTENT

#### Supporting Information

The Supporting Information is available free of charge at https://pubs.acs.org/doi/10.1021/acs.jpcc.0c10556.

TPD and AES spectra (PDF)

#### AUTHOR INFORMATION

## **Corresponding Author**

Andrew Teplyakov — Department of Chemistry and Biochemistry, University of Delaware, Newark, Delaware 19716, United States; orcid.org/0000-0002-6646-3310; Phone: (302) 831-1969; Email: andrewt@udel.edu; Fax: (302) 831-6335

#### **Authors**

Mahsa Konh – Department of Chemistry and Biochemistry, University of Delaware, Newark, Delaware 19716, United States

Anderson Janotti — Department of Material Science and Engineering, University of Delaware, Newark, Delaware 19716, United States; orcid.org/0000-0002-0358-2101

Complete contact information is available at: https://pubs.acs.org/10.1021/acs.jpcc.0c10556

#### Notes

The authors declare no competing financial interest.

#### ACKNOWLEDGMENTS

This work was partially supported by the National Science Foundation [DMR1609973 (GOALI) and CMMI2035354] and by the University of Delaware. A.J. acknowledges support from the NSF Early Career Award (grant no. DMR-1652994). The authors acknowledge the NSF (9724307 and 1428149) and the NIH NIGMS COBRE program (P30-GM110758) for partial support of activities in the University of Delaware Surface Analysis Facility. This work used the Extreme Science and Engineering Discovery Environment (XSEDE), 49 which is supported by the National Science Foundation (grant no. ACI-1548562). This work used the Extreme Science and Engineering Discovery Environment (XSEDE) Bridges GPU through allocation TG-CHE200089.

# REFERENCES

- (1) Kanarik, K. J.; Lill, T.; Hudson, E. A.; Sriraman, S.; Tan, S.; Marks, J.; Vahedi, V.; Gottscho, R. A. Overview of Atomic Layer Etching in the Semiconductor Industry. *J. Vac. Sci. Technol., A* **2015**, 33, 020802.
- (2) George, S. M.; Lee, Y. Prospects for Thermal Atomic Layer Etching Using Sequential, Self-Limiting Fluorination and Ligand-Exchange Reactions. *ACS Nano* **2016**, *10*, 4889–4894.
- (3) Manos, D.; Flamm, D. Plasma Etching: An Introduction; Elsevier,
- (4) Chen, J. K.-C.; Altieri, N. D.; Kim, T.; Lill, T.; Shen, M.; Chang, J. P. Directional Etch of Magnetic and Noble Metals. I. Role of Surface Oxidation States. *J. Vac. Sci. Technol., A* **2017**, *35*, 05C304.
- (5) Chen, J. K.-C.; Altieri, N. D.; Kim, T.; Chen, E.; Lill, T.; Shen, M.; Chang, J. P. Directional Etch of Magnetic and Noble Metals. II. Organic Chemical Vapor Etch. J. Vac. Sci. Technol., A 2017, 35, 05C305.
- (6) Abdulagatov, A. I.; George, S. M. Thermal Atomic Layer Etching of Silicon Nitride Using an Oxidation and "Conversion Etch" Mechanism. *J. Vac. Sci. Technol., A* **2020**, *38*, 022607.
- (7) Fan, Q.; Sang, L.; Jiang, D.; Yang, L.; Zhang, H.; Chen, Q.; Liu, Z. Plasma Enhanced Atomic Layer Deposition of Cobalt Nitride with Cobalt Amidinate. *J. Vac. Sci. Technol.*, A **2019**, *37*, 010904.
- (8) Kim, T.; Chen, J. K.-C.; Chang, J. P. Thermodynamic assessment and experimental verification of reactive ion etching of magnetic metal elements. *J. Vac. Sci. Technol., A* **2014**, 32, 041305.
- (9) Kim, T.; Kim, Y.; Chen, J. K.-C.; Chang, J. P. Viable Chemical Approach for Patterning Nanoscale Magnetoresistive Random Access Memory. *J. Vac. Sci. Technol., A* **2015**, 33, 021308.
- (10) Wang, Z.; Opila, R. L. In operando x-ray photoelectron spectroscopy study of mechanism of atomic layer etching of cobalt. *J. Vac. Sci. Technol., A* **2020**, *38*, 022611.
- (11) Konh, M.; He, C.; Lin, X.; Guo, X.; Pallem, V.; Opila, R. L.; Teplyakov, A. V.; Wang, Z.; Yuan, B. Molecular Mechanisms of Atomic Layer Etching of Cobalt with Sequential Exposure to Molecular Chlorine and Diketones. *J. Vac. Sci. Technol., A* **2019**, 37, 021004
- (12) Lin, X.; Chen, M.; Janotti, A.; Opila, R. In situ XPS study on atomic layer etching of Fe thin film using  $\text{Cl}_2$  and acetylacetone. J. Vac. Sci. Technol., A 2018, 36, 051401.
- (13) Park, S. D.; Lim, W. S.; Park, B. J.; Lee, H. C.; Bae, J. W.; Yeom, G. Y. Precise Depth Control and Low-Damage Atomic-Layer Etching of HfO<sub>2</sub> Using BCl<sub>3</sub> and Ar Neutral Beam. *Electrochem. Solid-State Lett.* **2008**, *11*, 71–74.
- (14) Min, K. S.; Kang, S. H.; Kim, J. K.; Yum, J. H.; Jhon, Y. I.; Hudnall, T. W.; Bielawski, C. W.; Banerjee, S. K.; Bersuker, G.; Jhon,

- M. S.; et al. Atomic layer etching of BeO using  $BCl_3/Ar$  for the interface passivation layer of III-V MOS devices. *Microelectron. Eng.* **2014**, 114, 121–125.
- (15) Mameli, A.; Verheijen, M. A.; Mackus, A. J. M.; Kessels, W. M. M.; Roozeboom, F. Isotropic Atomic Layer Etching of ZnO Using Acetylacetone and O<sub>2</sub> Plasma. *ACS Appl. Mater. Interfaces* **2018**, *10*, 38588–38595.
- (16) Lu, W.; Lee, Y.; Gertsch, J. C.; Murdzek, J. A.; Cavanagh, A. S.; Kong, L.; Del Alamo, J. A.; George, S. M. In Situ Thermal Atomic Layer Etching for Sub-5 Nm InGaAs Multigate MOSFETs. *Nano Lett.* **2019**, *19*, 5159–5166.
- (17) Lu, W.; Lee, Y.; Murdzek, J.; Gertsch, J.; Vardi, A.; Kong, L.; George, S. M.; Del Alamo, J. A. First Transistor Demonstration of Thermal Atomic Layer Etching: InGaAs FinFETs with Sub-5 Nm Fin-Width Featuring in Situ ALE-ALD. *Technical Digest—International Electron Devices Meeting, IEDM*; IEEE: San Francisco, CA, 2019; Vol. 2018-Decem, pp 39.1.1–39.1.4.
- (18) Lee, Y.; Dumont, J. W.; George, S. M. Mechanism of Thermal Al<sub>2</sub>O<sub>3</sub> Atomic Layer Etching Using Sequential Reactions with Sn(acac)<sub>2</sub> and HF. *Chem. Mater.* **2015**, *27*, 3648–3657.
- (19) Clancey, J. W.; Cavanagh, A. S.; Smith, J. E. T.; Sharma, S.; George, S. M. Volatile Etch Species Produced during Thermal Al<sub>2</sub>O<sub>3</sub> Atomic Layer Etching. *J. Phys. Chem. C* **2020**, *124*, 287–299.
- (20) Lee, Y.; George, S. M. Thermal Atomic Layer Etching of Al<sub>2</sub>O<sub>3</sub>, HfO<sub>2</sub>, and ZrO<sub>2</sub> Using Sequential Hydrogen Fluoride and Dimethylaluminum Chloride Exposures. *J. Phys. Chem. C* **2019**, 123, 18455.
- (21) Zhao, J.; Konh, M.; Teplyakov, A. Surface Chemistry of Thermal Dry Etching of Cobalt Thin Films Using Hexafluoroacety-lacetone (HfacH). *Appl. Surf. Sci.* **2018**, *455*, 438–445.
- (22) Zhu, J.-G. Magnetoresistive Random Access Memory: The Path to Competitiveness and Scalability. *Proc. IEEE* **2008**, *96*, 1786–1798
- (23) Dwyer, K. J.; Dreyer, M.; Butera, R. E. STM-Induced Desorption and Lithographic Patterning of Cl-Si(100)-(2  $\times$  1). *J. Phys. Chem. A* **2019**, *123*, 10793-10803.
- (24) Spencer, N. D.; Goddard, P. J.; Davies, P. W.; Kitson, M.; Lambert, R. M. A Simple, Controllable Source for Dosing Molecular Halogens in UHV. *J. Vac. Sci. Technol.*, A 1983, 1, 1554–1555.
- (25) Casa XPS; Casa Software Ltd: Teignmouth, U.K. 2010.
- (26) Frisch, M. J.; Trucks, G. W.; Schlegel, H. B.; Scuseria, G. E.; Robb, M. A.; Cheeseman, J. R.; Scalmani, G.; Barone, V.; Mennucci, B.; Petersson, G. A.; et al. *Gaussian 09*, Revision B.01.; Gaussian, Inc.: Wallingford CT, 2013.
- (27) Becke, A. D. A new mixing of Hartree-Fock and local density-functional theories. *J. Chem. Phys.* **1993**, 98, 1372–1377.
- (28) Lee, C.; Yang, W.; Parr, R. G. Development of the Colle-Salvetti Correlation-Energy Formula into a Functional of the Electron Density. *Phys. Rev. B: Condens. Matter Mater. Phys.* **1988**, 37, 785–789.
- (29) Ottonello, G.; Vetuschi Zuccolini, M. The Iron-Isotope Fractionation Dictated by the Carboxylic Functional: An Ab-Initio Investigation. *Geochim. Cosmochim. Acta* **2008**, *72*, 5920–5934.
- (30) Grimme, S.; Antony, J.; Ehrlich, S.; Krieg, H. A Consistent and Accurate Ab Initio Parametrization of Density Functional Dispersion Correction (DFT-D) for the 94 Elements H-Pu. *J. Chem. Phys.* **2010**, 132, 154104.
- (31) Kresse, G.; Joubert, D. From Ultrasoft Pseudopotentials to the Projector Augmented-Wave Method. *Phys. Rev. B: Condens. Matter Mater. Phys.* **1999**, *59*, 1758–1775.
- (32) Kresse, G.; Furthmüller, J. Efficient iterative schemes forab initiototal-energy calculations using a plane-wave basis set. *Phys. Rev. B: Condens. Matter Mater. Phys.* **1996**, *54*, 11169–11186.
- (33) Dudarev, S. L.; Botton, G. A.; Savrasov, S. Y.; Humphreys, C. J.; Sutton, A. P. Electron-Energy-Loss Spectra and the Structural Stability of Nickel Oxide: An LSDA+U Study. *Phys. Rev. B: Condens. Matter Mater. Phys.* 1998, *57*, 1505–1509.
- (34) Davey, W. P. Precision Measurements of the Lattice Constants of Twelve Common Metals. *Phys. Rev.* **1925**, *25*, 753–761.

- (35) Altarawneh, M.; Saraireh, S. A. Theoretical Insight into Chlorine Adsorption on the Fe(100) Surface. *Phys. Chem. Chem. Phys.* **2014**, *16*, 8575–8581.
- (36) Chase, M. W., Jr. NIST-JANAF Thermochemical Tables, 4th ed.; American Institute of Physics: New York, 1998.
- (37) Linsebigler, A. L.; Smentkowski, V. S.; Ellison, M. D.; Yates, J. T., Jr. Interaction of chlorine with iron(110) in the temperature range 90-1050 K. *J. Am. Chem. Soc.* **1992**, *114*, 465–473.
- (38) Linsebigler, A. L.; Smentkowski, V. S.; Yates, J. T., Jr. Interactional effects in corrosive chemisorption of chlorine and oxygen on iron(110). *Langmuir* 1992, *8*, 1950–1954.
- (39) Kuivila, C. S.; Butt, J. B.; Stair, P. C. Characterization of Surface Species on Iron Synthesis Catalysts by X-Ray Photoelectron Spectroscopy. *Appl. Surf. Sci.* **1988**, *32*, 99–121.
- (40) Grosvenor, A. P.; Kobe, B. A.; Biesinger, M. C.; McIntyre, N. S. Investigation of Multiplet Splitting of Fe 2p XPS Spectra and Bonding in Iron Compounds. *Surf. Interface Anal.* **2004**, *36*, 1564–1574.
- (41) Pierce, J. L.; Busch, K. L.; Cooks, R. G.; Walton, R. A. Desorption ionization mass spectrometry: secondary ion and laser desorption mass spectra of transition-metal complexes of .beta.-diketones. *Inorg. Chem.* **1982**, *21*, 2597–2602.
- (42) Sasaki, S.; Itagaki, Y.; Kurokawa, T.; Kasahara, A. Mass Spectrometric Studies of Metal Acetylacetonates. *Bull. Chem. Soc. Jpn.* **1967**, *40*, 76–80.
- (43) He, C.; Janzen, R.; Bai, S.; Teplyakov, A. V. "Clickable" Metal-Oxide Nanomaterials Surface-Engineered by Gas-Phase Covalent Functionalization with Prop-2-ynoic Acid. *Chem. Mater.* **2019**, *31*, 2068–2077.
- (44) He, P.; Ding, Z.; Zhao, X.; Liu, J.; Yang, S.; Gao, P.; Fan, L.-Z. Single-Crystal  $\alpha$ -Fe<sub>2</sub>O<sub>3</sub> with Engineered Exposed (001) Facet for High-Rate, Long-Cycle-Life Lithium-Ion Battery Anode. *Inorg. Chem.* **2019**, 58, 12724–12732.
- (45) Schönecker, S.; Li, X.; Johansson, B.; Kwon, S. K.; Vitos, L. Thermal Surface Free Energy and Stress of Iron. *Sci. Rep.* **2015**, 5, 14860.
- (46) Luo, Y. R. Comprehensive Handbook of Chemical Bond Energies; CRC Press: Boca Raton, FL, 2007.
- (47) Basher, A. H.; Krstić, M.; Fink, K.; Ito, T.; Karahashi, K.; Wenzel, W.; Hamaguchi, S. Formation and Desorption of Nickel Hexafluoroacetylacetonate Ni(Hfac)<sub>2</sub> on a Nickel Oxide Surface in Atomic Layer Etching Processes. *J. Vac. Sci. Technol., A* **2020**, 38, 052602.
- (48) Basher, A. H.; Krstić, M.; Takeuchi, T.; Isobe, M.; Ito, T.; Kiuchi, M.; Karahashi, K.; Wenzel, W.; Hamaguchi, S. Stability of Hexafluoroacetylacetone Molecules on Metallic and Oxidized Nickel Surfaces in Atomic-Layer-Etching Processes. *J. Vac. Sci. Technol., A* **2020**, 38, 022610.
- (49) Towns, J.; Cockerill, T.; Dahan, M.; Foster, I.; Gaither, K.; Grimshaw, A.; Hazlewood, V.; Lathrop, S.; Lifka, D.; Peterson, G. D.; et al. XSEDE: Accelerating Scientific Discovery. *Comput. Sci. Eng.* **2014**, *16*, 62–74.